ChemComm

COMMUNICATION

View Article Online
View Journal | View Issue

Cite this: *Chem. Commun.*, 2025, **61**, 1387

Received 27th July 2024,
Accepted 26th November 2024

DOI: 10.1039/d4cc03784g

rsc.li/chemcomm

Heterobimetallic contacts in statistical co-crystals of homoleptic coordination compounds with ligand-encoded H···F bonds: structure, photophysics and mechano-responsive properties†

Tobias Theiss, [ab] Stefan Buss, [ab] Iván Maisuls, [ab] Theresa Block,[a] Jutta Kösters,[a] Rainer Pöttgen [a] and Cristian A. Strassert [*ab]

In this work, the structural and photophysical characterization of statistical co-crystals based on two homoleptic Pt(II) and Pd(II) complexes as well as their mechano-responsive properties are reported. Ligand-dominated H···F bonds, which reinforce metal–metal interactions in the crystalline state, support emission from ^{3}MMLCT states. All co-crystals show a distinct red-shift upon grinding, showcasing their inherent mechano-responsive characteristics stemming from (hetero-)bimetallic contacts.

Due to their outstanding photophysical properties, transition metal complexes with 4d and 5d metal ions have been in the focus of research during the past decades. Possible areas of application for these compounds are optoelectronics,[1,2] cancer therapy,[3,4] bioimaging[5,6] and catalysis,[7,8] among many others. Such compounds involve metal ions with a d^6 electronic configuration (*e.g.*, Ir(III) or Re(I) centres, which typically present a (pseudo-)octahedral coordination geometry[9–11]) as well as (pseudo-)square-planar Au(III), Pt(II) and Pd(II) complexes with a d^8 configuration at the central atom. For the latter, the d_{z^2} orbitals of the metal ions protrude out of the coordination plane. The planar arrangements facilitate intermolecular interactions with electronic coupling of the central atoms from two adjacent coordination-chemical units, whereas the extent of intermolecular interactions depends on the judicious choice of ligands and microenvironment to support aggregation or excimer formation. While phosphorescence from metal-perturbed ligand-centered triplet states (^{3}MP-LC) can be observed for monomers, this emission primarily arises from the excited metal–metal-to-ligand charge-transfer (^{3}MMLCT) triplet states in dimeric units.[12,13] Complexes featuring bidentate[14,15] and tridentate[16,17] coordination environments have been extensively reported. In this sense, (bis-)cyclometalated ligands acting as tetradentate chromo-luminophores, offer particular photophysical advantages. The ligand-field splitting is enhanced by the two cyclometalated carbon atoms, which hampers non-radiative relaxation pathways. Moreover, these species have an increased rigidity, further preventing non-radiative deactivation processes.

In recent decades, there has been a growing interest in chelators that can bind different metal ions within the same molecule.[18,19] These mixed-metal compounds are used in a broad range of fields, including catalysis and cancer therapy. To date, however, there has been limited research on heterometallic complexes with homoleptic structure. Hence, metal ions would be coordinated in a similar fashion. Particularly when the metal ions share comparable ionic radii, compounds with emergent properties in solution and in the crystalline solid state can be realized. This appears plausible, for instance, when comparing Pt(II) and Pd(II) complexes, owing to the lanthanide contraction.[20,21] Hence, heterometallic analogues are usually prepared from a combination of different element classes.[22,23]

Herein, we report on the growth of statistical co-crystals based on two homoleptic Pt(II) and Pd(II) complexes, which are isostructural both in solution and in the crystalline state. The molecular structures of the pure compounds, [**PtL**] and [**PdL**], are shown in Fig. 1A. Studies on the structural and photophysical properties as well as (TD)DFT-based computational calculations regarding the two individual compounds have already been reported by our group, showing that H···F bonds support Pd–Pd and Pt–Pt interactions.[24]

The term co-crystal has repeatedly been discussed with respect to its expressiveness[25,26] and also the term multi-component molecular crystal has been introduced. Our crystallization experiments fulfil these requirements. The two components for crystallization are [**PtL**] and [**PdL**], which are finally dimerized in a statistical manner (missing long-range order) and we consequently call these product phases statistical

[a] *Institut für Anorganische und Analytische Chemie, Universität Münster, Corrensstraße 28/30, 48149 Münster, Germany. E-mail: ca.s@uni-muenster.de*
[b] *CiMIC, SoN, CeNTech, Universität Münster, Heisenbergstraße 11, 48149 Münster, Germany*

† Electronic supplementary information (ESI) available: Additional crystallographic and photophysical data. CCDC 2300665, 2303661 and 2303662. For ESI and crystallographic data in CIF or other electronic format see DOI: https://doi.org/10.1039/d4cc03784g

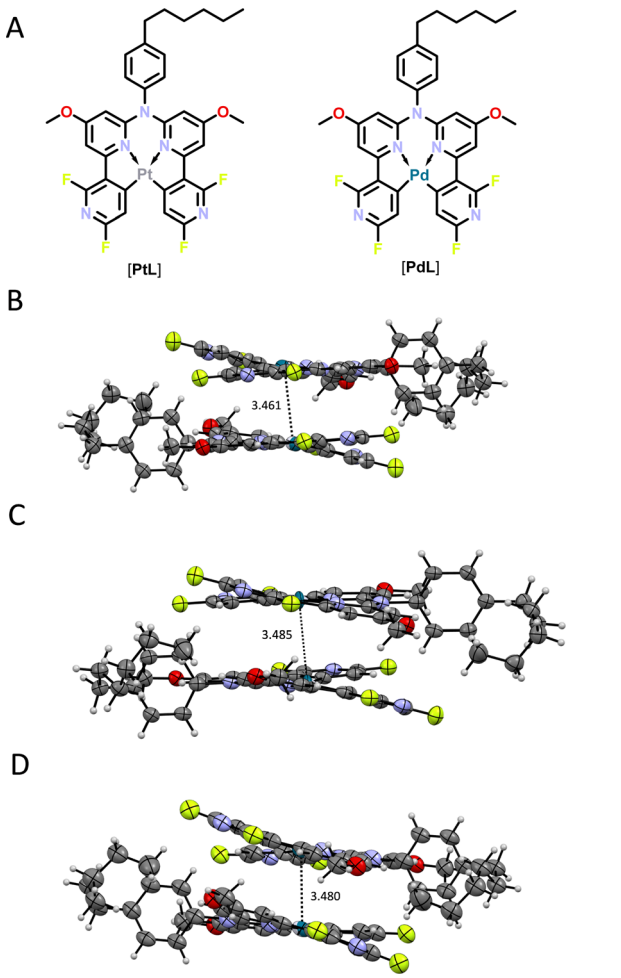

Fig. 1 (A) Structural formulae of the pure compounds ([**PtL**] and [**PdL**]).[24] (B) Molecular structure in the statistical co-crystal with the ratio [**PtL**][**PdL**] 3 : 1. (C) Molecular structure in the statistical co-crystal with the ratio [**PtL**][**PdL**] 1 : 1. (D) Molecular structure in the statistical co-crystal with the ratio [**PtL**][**PdL**] 1 : 3. The metal–metal distances are given in Ångstrom (Å).

co-crystals. To achieve such statistical co-crystals with varying compositions regarding the complexes, solutions of the compounds in the ratios 1 : 1, 1 : 3 and 3 : 1 (n : n) were mixed and single crystals were obtained by slow evaporation of the solvent. The molecular structures in the statistical co-crystals were obtained from X-ray diffraction data (see Fig. 1B–D as well as Fig. S1–S7 in the ESI†), and their composition was confirmed, within the experimental uncertainty, by micro-X-ray fluorescence spectroscopic (μXRF) analysis (see Table S1, ESI†).

Like previously reported for the pure complexes [**PtL**] and [**PdL**], the three statistical co-crystals show a head-to-tail arrangement of the dimers in the asymmetric unit. This is due to the formation of ligand-encoded H···F bridges that support the aforementioned metal–metal coupling between the d^8-configured cations. The distances between the metal centers in a dimer fall in the typical range for metal–metal interactions (<3.5 Å).

The co-crystallization experiments of the individual [**PtL**] and [**PdL**] complexes can induce ordering within the crystal structure. Exemplarily we discuss the possibilities for the 1 : 1 ratio of [**PtL**][**PdL**]. Since our X-ray diffraction experiments gave no hints for primitive reflections, only the two *translationengleiche* subgroups *Cc* and *C*2 were considered. It is thus clear that [**PtL**]/[**PdL**] ordering leads to a loss of the inversion center between the two complex entities.

The decoupling of the positional parameters proceeds in two different ways, thus affecting the four dumbbells within one unit cell (Fig. S1, ESI†). In subgroup *Cc,* [**PtL**]/[**PdL**] ordering occurs within each dumbbell with exactly the same alignment. A switch in alignment would require a further symmetry reduction to a space group with a *P* lattice, which is unlikely in the present case, since no *P* reflections were observed. The ordering pattern is different in space group *C*2. Here we retain two individual Pt_2 and Pd_2 dumbbells per unit cell.

A look at the crystallographic data collected for [**PtL**][**PdL**] crystals of compositions 3 : 1, 1 : 1 and 1 : 3 (Tables S2–S4, ESI†) shows only a tiny influence of the composition on the lattice parameters. This is a clear consequence of the almost identical size of the Pt^{2+} and Pd^{2+} cations (relativistic contraction of platinum). The small differences within the platinum *vs.* palladium coordination requirements is then expressed in tiny changes in the atomic coordinates (Table S2, ESI†) and slightly enhanced displacement parameters (Table S3, ESI†).

The three crystals studied herein gave no hint for long-range [**PtL**]/[**PdL**] ordering. Nevertheless, refinements of the occupancy parameters fully reflected the starting compositions of the crystallization experiments. Thus, only short-range order is present in the samples. Besides the Pt–Pd dumbbells, especially in the 1 : 3 and 3 : 1 samples we observe a large amount of Pt_2 and Pd_2 dumbbells. Therefore, the lack of long-range order justifies to call the present species statistical co-crystals.

In addition to the structural investigation of the three co-crystals, photophysical experiments were performed in solution and for the crystalline solids, both at room temperature and in a frozen glassy matrix at 77 K (Fig. S8–S13 and Table S5, ESI†). In frozen DCM/MeOH, 1 : 1 at 77 K (Fig. S11, ESI†), a red shift was observed as the proportion of the Pt(II) complex increased. The emission maximum for the pure [**PdL**] species is found at 525 nm, whereas [**PtL**] displays a peak centered at 596 nm.[24] The emission maxima of the three statistical co-crystals fall in between these two values. Furthermore, it can be shown that metal–metal interactions are inducible in a targeted manner: At 77 K, the choice of the glassy matrix strongly influences aggregation. Hence, our previous work demonstrated that metal–metal interactions are supported by a frozen glassy matrix consisting of MeOH and DCM, but suppressed in 2-Me-THF. With progressively longer excitation wavelengths, higher aggregates can be addressed in dilute glasses at 77 K, resulting in distinct emission profiles (see Fig. S8–S10, ESI†). This property is also evident in concentrated liquid solutions (10^{-3} M) at room temperature when the [**PtL**]**PdL**] ratio is 1 : 1 (Fig. S12, ESI†). In the crystalline state, the four (co-)crystals (with Pt(II) complex contents ranging from 25% to 100%) exhibit a broad yet unstructured emission band symmetrically centered at around 588 nm (Fig. 3 and Fig. S14, ESI†), which points towards metal–metal coupling mediated by the rather

diffuse $5d_{z^2}$ orbitals while leading to an intermolecularly delocalized excited state. The emission spectrum from the crystalline sample of the pure [**PdL**] species deviates from this behavior: Its emission maximum is blue-shifted compared to the crystals containing [**PtL**] (λ_{max} = 528 nm), and the spectrum shows a vibrational shoulder at 565 nm, indicating a ligand-dominated emission. This differs from the pure monomer, which is red-shifted due to short intermolecular distances that promote excimeric excited-state character. Upon mechanical grinding of the five crystalline samples, all emission spectra exhibit a comparable profile and shape, characterized by broad and unstructured maxima (Fig. 3 and Fig. S15, ESI†). Much like at 77 K (*vide supra*), a red shift becomes evident with growing contents of Pt(II) units. While the emission maximum of [**PdL**] in the solid state is located at λ_{max} = 531 nm and for [**PtL**] at λ_{max} = 720 nm, the maxima of the three co-crystals fall in between the range of the pure species.

Additionally, the mechanoresponsive properties of the five crystalline samples were explored using photoluminescence lifetime imaging micro(spectro)scopy (PLIM, as illustrated in Fig. 2 as well as Fig. S16–S19, ESI†). Hence, shear forces were applied to the samples by mechanical grinding. Micrographs were acquired for both the crystalline and ground complexes (Fig. 2), and the spatiotemporally resolved emission spectra were investigated both before and after grinding. As depicted in Fig. S16 and S17 (ESI†), prior to the exertion of shearing forces, all samples with a Pt(II) ratio between 25% and 75% exhibit a broad, unstructured signal that peaks at approximately λ_{max} = 580 nm. In contrast, the spectrum of the Pd(II) crystal displays a characteristic vibrational progression with a maximum of λ_{max} = 525 nm as well as vibronic shoulders at λ = 565 nm and λ = 610 nm. This suggests that in the intact palladium-based crystal, the emission primarily originates from ligand-centered states with intermolecular coupling (*vide supra*). After grinding, all crystals containing Pt(II) show a clear red shift of up to 90 nm, as shown in Fig. S16 and S17 (ESI†). Interestingly, the color of [**PdL**] remained unaltered, with no traceable red shift upon grinding. However, post-grinding, the spectrum of the pure Pd(II)-based crystal no longer exhibits a vibronic structure but rather manifests as a broadly unstructured profile, which despite appearing blue shifted strongly resembles the emission spectra of the other four samples.

This observation implies that upon grinding, the emission occurs from states with enhanced ^{3}MMLCT character, where the metal–metal coupling is stronger for the diffuse $5d_{z^2}$ orbitals than for their $4d_{z^2}$ counterparts. In fact, upon grinding, the deep-red emission is dominated by the Pt(II) centres, which appears orange- or green-shifted with 75% or 100% palladium content, respectively. In the spatiotemporally-resolved spectra of all samples, the lifetime maps upon grinding display a change of the excited state character with local inhomogeneities, as the shortened lifetimes and red-shifts vary as a function of space (Fig. S18 and S19, ESI†). Moreover, powder X-ray diffraction measurements of [**PtL**], [**PdL**] as well as [**PtL**][**PdL**] 1 : 3 and [**PtL**][**PdL**] 3 : 1 confirm a phase transition from crystalline to amorphous solid upon grinding (Fig. S20–S23, ESI†).

In summary, we prepared three samples of statistical co-crystals with heterobimetallic contacts, starting from the pure Pt(II) and Pd(II) coordination compounds, namely [**PtL**] and [**PdL**]. The statistical distribution of the different metal centres was probed by single crystal X-ray diffraction experiments. Metal–metal distances below 3.5 Å were observed for all co-crystals. Further photophysical studies were carried out for the mixtures in solution and in a frozen glassy matrix, as well as in the crystalline state. Tuneable emissive behaviour is observed in the solid state as well as in frozen matrices at 77 K: The higher the ratio of Pt(II), the stronger is the observed red shift of the emission. After applying shear forces on the five crystalline samples, a responsive behaviour with memory of mechanical stress was observed, providing dual macro- and microscopic readouts (lifetime changes and spectral shifts). Ongoing studies are focussed on other forms of external stimuli to gain a deeper understanding of the emerging properties from increasingly complex systems.

C. A. S. acknowledges funding from the Deutsche Forschungsgemeinschaft (DFG, German Research Foundation)

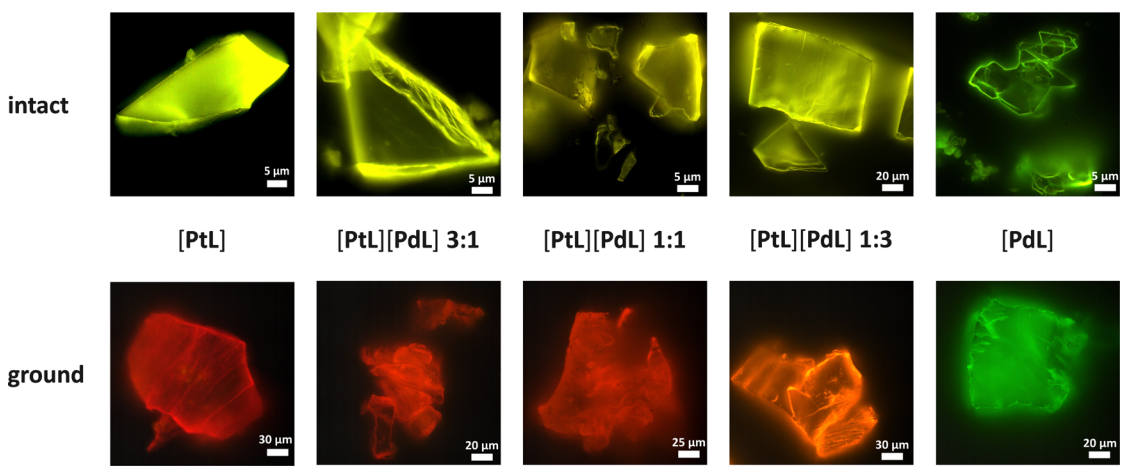

Fig. 2 Micrographs of [**PtL**],[24] [**PdL**][24] and their statistical co-crystals with different compositions before (top) and after (bottom) grinding.

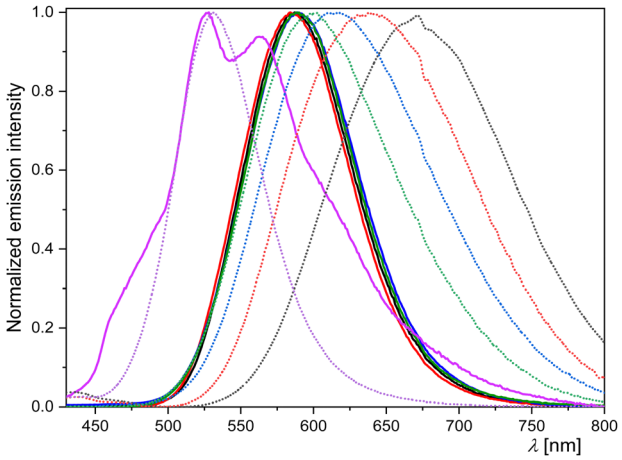

Fig. 3 Emission spectra of [**PtL**] (black), [**PtL**][**PdL**] 3 : 1 (red), [**PtL**][**PdL**] 1 : 1 (blue), [**PtL**][**PdL**] 1 : 3 (green), [**PdL**] (magenta) as crystalline solids (solid lines) and as ground solids (dashed lines). λ_{exc} = 376 nm, 298 K.

– Project-ID 433682494 – SFB 1459 "Intelligent Matter" and Project STR 1186/6-2 within the Priority Programm 2102 "Light-controlled reactivity of metal complexes". C. A. S. is grateful for the support to acquire an "Integrated Confocal Luminescence Spectrometer with Spatiotemporal Resolution and Multiphoton Excitation" (DFG/Land NRW: INST 211/915-1 FUGG; DFG EXC1003: "Berufungsmittel"). We thank Prof. Dr. Uwe Karst and Michael Holtkamp for their help with the μXRF measurements.

Data availability

The data supporting this article have been included as part of the ESI.† Crystallographic data for all crystal structures has been deposited at the CCDC under the numbers 2300665, 2303661 and 2303662.

Conflicts of interest

There are no conflicts to declare.

References

1 M.-C. Tang, M.-Y. Chan and V. W.-W. Yam, *Chem. Rev.*, 2021, **121**, 7249–7279.
2 G. Zhou, W.-Y. Wong and X. Yang, *Chem. – Asian J.*, 2011, **6**, 1706–1727.
3 S. Dasari and P. B. Tchounwou, *Eur. J. Pharmacol.*, 2014, **740**, 364–378.
4 U. Ndagi, N. Mhlongo and M. E. Soliman, *Drug Des., Dev. Ther.*, 2017, **11**, 599–616.
5 Q. Zhao, C. Huang and F. Li, *Chem. Soc. Rev.*, 2011, **40**, 2508–2524.
6 K. K.-W. Lo and K. Y. Zhang, *RSC Adv.*, 2012, **2**, 12069.
7 Z. Liu and P. J. Sadler, *Acc. Chem. Res.*, 2014, **47**, 1174–1185.
8 A. Bolje, S. Hohloch, M. van der Meer, J. Košmrlj and B. Sarkar, *Chem. – Eur. J.*, 2015, **21**, 6756–6764.
9 B. Happ, A. Winter, M. D. Hager and U. S. Schubert, *Chem. Soc. Rev.*, 2012, **41**, 2222–2255.
10 T. U. Connell and P. S. Donnelly, *Coord. Chem. Rev.*, 2018, **375**, 267–284.
11 V. Fernández-Moreira, F. L. Thorp-Greenwood and M. P. Coogan, *Chem. Commun.*, 2010, **46**, 186–202.
12 I. Maisuls, C. Wang, M. E. Gutierrez Suburu, S. Wilde, C.-G. Daniliuc, D. Brünink, N. L. Doltsinis, S. Ostendorp, G. Wilde, J. Kösters, U. Resch-Genger and C. A. Strassert, *Chem. Sci.*, 2021, **12**, 3270–3281.
13 I. Maisuls, F. Boisten, M. Hebenbrock, J. Alfke, L. Schürmann, B. Jasper-Peter, A. Hepp, M. Esselen, J. Müller and C. A. Strassert, *Inorg. Chem.*, 2022, **61**, 9195–9204.
14 J. Soellner, P. Pinter, S. Stipurin and T. Strassner, *Angew. Chem., Int. Ed.*, 2021, **60**, 3556–3560.
15 M. Nazish, M. M. Siddiqui, S. Kumar Sarkar, A. Münch, C. M. Legendre, R. Herbst-Irmer, D. Stalke and H. W. Roesky, *Chem. – Eur. J.*, 2021, **27**, 1744–1752.
16 D. Ravindranathan, D. A. K. Vezzu, L. Bartolotti, P. D. Boyle and S. Huo, *Inorg. Chem.*, 2010, **49**, 8922–8928.
17 Y. Chi, T.-K. Chang, P. Ganesan and P. Rajakannu, *Coord. Chem. Rev.*, 2017, **346**, 91–100.
18 F. G. Baddour, S. R. Fiedler, M. P. Shores, J. W. Bacon, J. A. Golen, A. L. Rheingold and L. H. Doerrer, *Inorg. Chem.*, 2013, **52**, 13562–13575.
19 S. Kuppuswamy, T. R. Cass, M. W. Bezpalko, B. M. Foxman and C. M. Thomas, *Inorg. Chim. Acta*, 2015, **424**, 167–172.
20 M.-H. Huang, W.-Y. Lee, X.-R. Zou, C.-C. Lee, S.-B. Hong and L.-C. Liang, *Appl. Organomet. Chem.*, 2021, 35.
21 I. S. Puchtel, in *Encyclopedia of Geochemistry*, ed. W. M. White, Springer International Publishing, Cham, 2016, 1–5.
22 E. V. Dikarev, H. Zhang and B. Li, *J. Am. Chem. Soc.*, 2005, **127**, 6156–6157.
23 T. L. Sunderland and J. F. Berry, *Dalton Trans.*, 2016, **45**, 50–55.
24 T. Theiss, S. Buss, I. Maisuls, R. López-Arteaga, D. Brünink, J. Kösters, A. Hepp, N. L. Doltsinis, E. A. Weiss and C. A. Strassert, *J. Am. Chem. Soc.*, 2023, **145**, 3937–3951.
25 D. Bond, *CrystEngComm*, 2007, **9**, 833–834.
26 S. Aitipamula, R. Banerjee, A. K. Bansal, K. Biradha, M. L. Cheney, A. R. Choudhury, G. R. Desiraju, A. G. Dikundwar, R. Dubey, N. Duggirala, P. P. Ghogale, S. Gosh, P. K. Goswami, N. R. Goud, R. R. K. R. Jetti, P. Karpinski, P. Kaushik, D. Kumar, V. Kumar, B. Moulton, A. Mukherjee, A. S. Myerson, V. Puri, A. Ramanan, T. Rajamannar, C. M. Reddy, N. Rodriguez-Hornedo, R. D. Rogers, T. N. Guru Row, P. Sanphui, N. Shan, G. Shete, A. Singh, C. C. Sun, J. A. Swift, R. Thaimattam, T. S. Thakur, R. K. Thaper, S. P. Thomas, S. Tothadi, V. R. Vangala, N. Variankaval, P. Vishweshwar, D. R. Weyna and M. J. Zaworotko, *Cryst. Growth Des.*, 2012, **12**, 2147–2152.

